Abstract #00385 ISMRM ABSTRACT

[USGOV] Simultaneous real-time NMR and microscopy for validation of diffusion microstructure biomarkers

Primary: Diffusion - Microstructure 〉 **Secondary:** Diffusion - Simulation/Validation 〉 **Keywords:** DOUBLE DIFFUSION ENCODING DEXSY VITAL SIGNS MONITORING LOW-FIELD PORTABLE WATER EXCHANGE RATE

Nathan H Williamson [1,2,3], **Rea Ravin**[2,4], **Teddy X Cai**[2], **Peter J Basser**[2]

[1]The Henry M. Jackson Foundation for the Advancement of Military Medicine, Inc., Bethesda, United States of America
[2]Section on Quantitative Imaging and Tissue Sciences (SQITS), Eunice Kennedy Shriver - National Institute of Child Health and Human Development (NICHD), Bethesda, United States of America
[3]Uniformed Services University of the Health Sciences, Bethesda, United States of America
[4]Celoptics, Rockville, United States of America

Presenting Author: *Nathan H Williamson (williamsonnh@nih.gov)*

Impact

Simultaneous real-time NMR and microscopy reveal how diffusion and exchange metrics respond to osmotic and ionic challenges in viable ex vivo neural tissue, enabling direct validation of MRI-based microstructural biomarkers and bridging the gap between neurophysiology and radiological measurements.

Synopsis

Motivation: Diffusion MRI reflects tissue microstructure and function, but direct validation in living neural tissue remains challenging.
Goals: To combine microscopy and NMR for real-time recording on viable ex vivo neural tissue during cellular perturbations.
Approach: Simultaneous high-temporal-resolution NMR and optical microscopy were used to monitor diffusion (ADC), exchange (AXR), intrinsic optical signal (IOS), and intracellular calcium ($[\mathrm{Ca}^{2+}]_i$) in ex vivo neonatal mouse spinal cord during osmotic and ionic perturbations.
Results: ADC strongly correlated with IOS, while AXR decreased with depolarization. ADC and AXR were sensitive to distinct aspects of cellular swelling, supporting their complementary roles in probing tissue viability and function.

Introduction

In vivo diffusion and exchange MRI have demonstrated sensitivity to cellular physiology and pathology [1–6], but validation efforts can be confounded by hemodynamics [7], physiological noise [8], and limited compatibility with optical modalities [9,10]. Viable ex vivo tissue models provide an alternative, allowing cellular physiology and pathology to be studied in isolation and in combination with optical microscopy [11].

Using this approach, here high-temporal-resolution NMR measurements of apparent diffusion coefficients (ADC) and apparent exchange rates (AXR) are paired with intrinsic optical signal (IOS) microscopy and intracellular calcium ($[\mathrm{Ca}^{2+}]_i$) to track microstructural and functional changes during ionic and osmotic perturbations. Strong correlations with IOS confirm ADC's sensitivity to cellular swelling and shrinking. AXR appears to change only during perturbations which induce loss of tissue viability, seen by $[\mathrm{Ca}^{2+}]_i$ spiking, supporting the hypothesis that AXR is sensitive to tissue viability [12].

Methods

Neonatal mouse spinal cords (P1–P4) were dissected and maintained viable at 25°C in circulating oxygenated artificial cerebrospinal fluid (aCSF). NMR data were acquired at 13.79 MHz using a low-field single-sided permanent magnet (Magritek NMR MOUSE) and custom solenoid RF coil and test chamber, while simultaneous optical imaging was performed every 30 s through a gap in the coil using an Axiovert 200 M microscope (Zeiss) and an objective inverter (LSMtech) (Fig. 1).

Diffusion encoding was performed along the y -axis on sub-millisecond timescales by RF pulses modulating the effect of a large ($g = 15.3$ T/m) static gradient (SG) [13]. ADC was estimated from two SG spin echo (SE) diffusion-weighted signals, $S(1)$ and $S(2)$ at $b(1) = 0.025$ and $b(2) = 2.25\ \mathrm{ms}/\mu\mathrm{m}^2$, using

$$\mathrm{ADC} = -\frac{1}{b(1) - b(2)} \ln \frac{S(2)}{S(1)}, \qquad (1)$$

where $b = \frac{2}{3}\gamma^2 g^2 \tau^3$.

SG diffusion exchange spectroscopy (DEXSY) [13-15] signals were acquired with $(b_1, b_2) = (2.32, 2.17)\ \mathrm{ms}/\mu\mathrm{m}^2$ and mixing times $t_m =$ 0.2, 10, 160 ms which are short, intermediate, and long relative to $1/\mathrm{AXR}$. The signals were then corrected for longitudinal relaxation and then combined as

$$\mathrm{AXR} = -\frac{1}{t_{m,\mathrm{int}}} \ln \left(1 - \frac{S_{\mathrm{short}} - S_{\mathrm{int}}}{S_{\mathrm{short}} - S_{\mathrm{long}}} \right). \qquad (2)$$

IOS was obtained from transmitted near-infrared 680 nm light [15]. For $[Ca^{2+}]_i$ imaging, tissues were loaded with a bolus injection of Rhod-3 AM fluorescent indicator (ThermoFisher). Signals from a region of interest were expressed as percent signal change from baseline.

IOS microscopy and NMR were recorded simultaneously during 40 minute perturbations with 100 mM sucrose (an osmolyte). $[Ca^{2+}]_i$ was recorded in addition to IOS and NMR during 20 minute perturbations with 50 mM KCl.

Results and discussion

Example recordings from a 50 mM KCl perturbation experiment are shown in Fig. 2. Raw signals from two SG SE and three SG DEXSY acquisitions were processed into ADC and AXR using Eqs. 1 and 2, respectively (Fig. 2a–d). Each signal represents summed echoes from the CPMG acquisition block, from which phase and transverse relaxation rates (R_2) were also derived (Fig. 2e,f). Phase reflects ionic composition and shows rapid equilibration after KCl addition (~1 min) and slower recovery during washout (~10 min), likely limited by K^+ efflux. Its independence from diffusion weighting confirms negligible coherent flow. R_2 increased with diffusion weighting, consistent with faster relaxation in restricted environments, and showed distinct time courses: R_2 declined steadily, while diffusion-weighted R_2 dropped mainly during washout. Although noteworthy, the following analysis focuses on ADC and AXR. NMR data were acquired simultaneously with IOS and $[Ca^{2+}]_i$ imaging (Fig. 2 g,h); during washout, $[Ca^{2+}]_i$ fell below baseline, likely as dye diffused from the region of interest.

In 100 mM sucrose, ADC and IOS increase due to cellular shrinkage. AXR increases significantly ($p = 0.002$), but the effect is small. The small effect on AXR is consistent with homeostasis being maintained.

In 50 mM KCl, $[Ca^{2+}]_i$ spiked within 3 min, indicating spreading depolarization, followed by decreases in IOS and ADC, consistent with swelling induced by spreading depolarization. AXR dropped at the same time as ADC and IOS and partially recovered during washout, but remained below baseline.

Across experiments, ADC and IOS correlated strongly during osmotic and depolarizing conditions, consistent with sensitivity to cell volume changes, while AXR showed independent trends.

These results demonstrate that real-time NMR–microscopy integration can capture coupled microstructural and physiological dynamics to directly validate the sensitivity of diffusion MRI metrics to cell structure and function. ADC and AXR provide complementary readouts of diffusion and transmembrane exchange, with AXR capturing distinct effects consistent with tissue viability.

Acknowledgements

This research was supported [in part] by the Intramural Research Program of the National Institutes of Health (NIH). This work was partially funded by the Department of War in the Military Traumatic Brain Injury Initiative under award HU0001-24-2-0051.

References

1. Helene Benveniste, Laurence W Hedlund, and G Allan Johnson. Mechanism of detection of acute cerebral ischemia in rats by diffusion-weighted magnetic resonance microscopy. Stroke, 23(5):746–754, 1992. https://doi.org/10.1161/01.STR.23.5.746

2. Lawrence L Latour, Yasuhiro Hasegawa, James E Formato, Marc Fisher, and Christopher H Sotak. Spreading waves of decreased diffusion coefficient after cortical stimulation in the rat brain. Magnetic resonance in medicine, 32(2):189–198, 1994. https://doi.org/10.1002/mrm.1910320207

3. Denis Le Bihan, Shin-ichi Urayama, Toshihiko Aso, Takashi Hanakawa, and Hidenao Fukuyama. Direct and fast detection of neuronal activation in the human brain with diffusion mri. Proceedings of the National Academy of Sciences, 103(21):8263–8268, 2006. https://doi.org/10.1073/pnas.0600644103

4. Daniel Nunes, Andrada Ianus, and Noam Shemesh. Layer-specific connectivity revealed by diffusion-weighted functional mri in the rat thalamocortical pathway. Neuroimage, 184: 646–657, 2019. https://doi.org/10.1016/j.neuroimage.2018.09.050

5. Inès de Riedmatten, Arthur PC Spencer, Wiktor Olszowy, and Ileana O Jelescu. Apparent diffusion coefficient fmri shines light on white matter resting-state connectivity compared to bold. Communications biology, 8(1):447, 2025. https://doi.org/10.1038/s42003-025-07889-0

6. Andreea Hertanu, Tommaso Pavan, Ileana O. Jelescu; Somatosensory-evoked response induces extensive diffusivity and kurtosis changes associated with neural activity in rodents. Imaging Neuroscience, 2025. https://doi.org/10.1162/imag_a_00445

7. Karla L Miller, Daniel P Bulte, Hannah Devlin, Matthew D Robson, Richard G Wise, Mark W Woolrich, Peter Jezzard, and Timothy EJ Behrens. Evidence for a vascular contribution to diffusion fmri at high b value. Proceedings of the National Academy of Sciences, 104(52): 20967–20972, 2007. https://doi.org/10.1073/pnas.0707257105

8. . Kulam Najmudeen Magdoom, Alexandru V Avram, Joelle E Sarlls, and Peter J Basser. In vivo palpation of anisotropic human brain tissue using mri. bioRxiv, pages 2025–06, 2025. https://doi.org/10.1101/2025.06.20.660588

9. . Meng Cui, Yifeng Zhou, Bowen Wei, Xiao-Hong Zhu, Wei Zhu, Mark A Sanders, Kamil Ugurbil, and Wei Chen. A proof-of-concept study for developing integrated two-photon microscopic and magnetic resonance imaging modality at ultrahigh field of 16.4 tesla. Scientific reports, 7(1):2733, 2017. https://doi.org/10.1038/s41598-017-02864-0

10. Evelyn MR Lake, Xinxin Ge, Xilin Shen, Peter Herman, Fahmeed Hyder, Jessica A Cardin, Michael J Higley, Dustin Scheinost, Xenophon Papademetris, Michael C Crair, et al. Simultaneous cortex-wide fluorescence ca2+ imaging and whole-brain fmri. Nature methods, 17 (12):1262–1271, 2020. https://doi.org/10.1038/s41592-020-00984-6

11. Ruiliang Bai, Andreas Klaus, Tim Bellay, Craig Stewart, Sinisa Pajevic, Uri Nevo, Hellmut Merkle, Dietmar Plenz, and Peter J Basser. Simultaneous calcium fluorescence imaging and mr of ex vivo organotypic cortical cultures: a new test bed for functional mri. NMR in Biomedicine, 28(12):1726–1738, 2015. https://doi.org/10.1002/nbm.3424

12. Nathan H Williamson, Rea Ravin, Teddy X Cai, Melanie Falgairolle, Michael J O'Donovan, and Peter J Basser. Water exchange rates measure active transport and homeostasis in neural tissue. PNAS nexus, 2(3), 2023. https://doi.org/10.1093/pnasnexus/pgad056

13. Nathan H Williamson, Rea Ravin, Dan Benjamini, Hellmut Merkle, Melanie Falgairolle, Michael James O'Donovan, Dvir Blivis, Dave Ide, Teddy X Cai, Nima S Ghorashi, et al. Magnetic resonance measurements of cellular and sub-cellular membrane structures in live and fixed neural tissue. Elife, 8:e51101, 2019. https://doi.org/10.7554/eLife.51101

14. Nathan H Williamson, Rea Ravin, Teddy X Cai, Dan Benjamini, Melanie Falgairolle, Michael J O'Donovan, and Peter J Basser. Real-time measurement of diffusion exchange rate in biological tissue. Journal of Magnetic Resonance, 317:106782, 2020. https://doi.org/10.1016/j.jmr.2020.106782

15. P. T. Callaghan and I. Furó. Diffusion-diffusion correlation and exchange as a signature for local order and dynamics. The Journal of Chemical Physics, 120(8):4032–4038, 2004. https://doi.org/10.1063/1.1642604

16. Eva Syková, Lydia Vargová, Sárka Kubinová, Pavla Jendelová, and Alexandr Chvátal. The relationship between changes in intrinsic optical signals and cell swelling in rat spinal cord slices. Neuroimage, 18(2):214–230, 2003. https://doi.org/10.1016/s1053-8119(02)00014-9

Figures and Tables

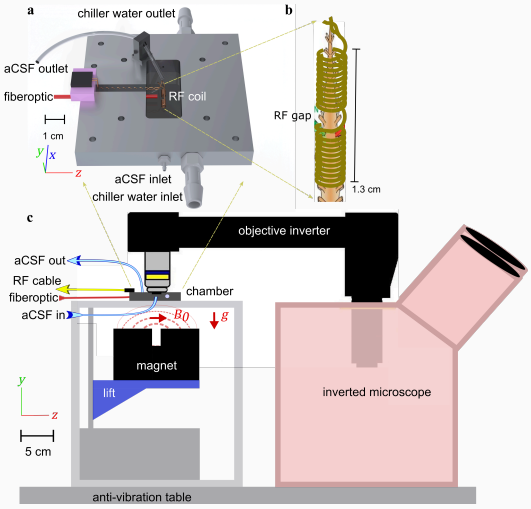

Figure 1: Experimental setup *a) 3-D technical drawing of the test chamber. b) Drawing of the solenoid RF coil containing a mouse spinal cord showing the gap in the RF coil where the sample is imaged. c) Technical drawing of the experimental setup showing the single sided permanent magnet projecting a magnetic field on the sample from below and the inverted microscope imaging the sample from above.*

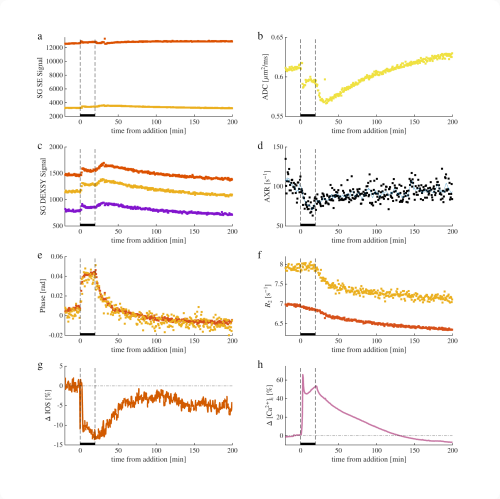

Figure 2: Example NMR and microscopy recordings during 50 mM KCl addition and washout. *a,b) Two SE signals ($b(1)=0.025$, $b(2)=2.25\ \mathrm{ms/\mu m^2}$) yield ADC. c,d) Three DEXSY signals ($t_m=$0.2, 10, 160 ms) yield AXR. Blue line in (d) shows 6-point average. e,f) CPMG echo phase and R_2 weighted by $b(1)$ (red) and $b(2)$ (orange). g,h) % change in ROI intensity from IOS and $\mathrm{[Ca^{2+}]_i}$ images.*

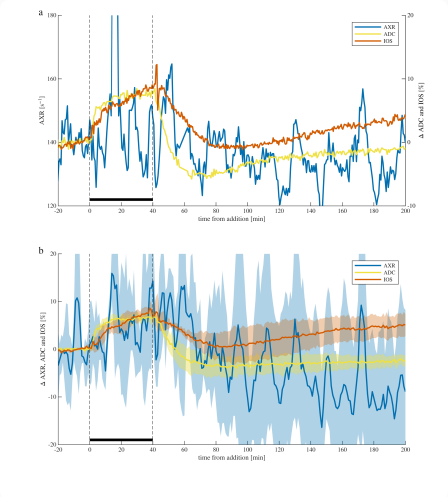

Figure 3: Simultaneous real-time NMR and microscopy shows cellular shrinkage caused by adding an osmolyte*. a) A representative sample and b) means (lines) and standard deviations (shaded bands) across n=4 samples of real-time AXR (6-point moving average), ADC, and IOS recording during experiments involving 100 mM sucrose being added for 40 minutes and then washed away.*

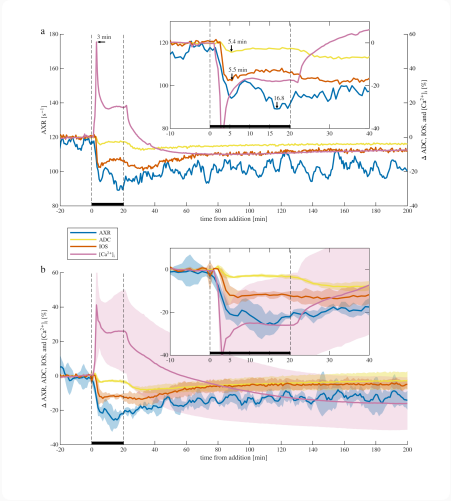

Figure 4: Simultaneous real-time NMR and microscopy reveal cellular swelling during depolarization from 50 mM KCl*. a) Representative sample and b) mean ± SD (n = 3) of AXR (6-point moving average), ADC, IOS, and $\mathrm{[Ca^{2+}]_i}$ during 20 min KCl exposure and washout. Insets show zoomed regions with $\mathrm{[Ca^{2+}]_i}$ inverted for comparison. Arrows in (a) mark signal minima and maxima.*